VIP Selective Heteroepitaxy

DOI: 10.1002/anie.201203069

Selective Heteroepitaxial Nanocrystal Growth of Rare Earth Fluorides on Sodium Chloride: Synthesis and Density Functional Calculations**

Feng Wang, Ling-Dong Sun, Jun Gu, Ye-Fu Wang, Wei Feng, Yi Yang, Jianfang Wang,* and Chun-Hua Yan**

Colloidal heteronanocrystals have drawn tremendous attention in the last decade because they offer unlimited possibilities in either promoting properties of their individual components or integrating various functional components within one single structure.[1–9] These tunable properties lead to potential applications in diverse fields, such as catalytic reactions,[10–12] solar energy harvesting,[13,14] optoelectronics,[15,16] upconversion emission,[17] and biological applications.[18] A thorough understanding of their growth mechanism is required to optimize their performance in various applications. Most colloidal heteronanocrystals are synthesized through epitaxial growth. Previous studies used the growth model of multilayered thin films to illustrate the epitaxial growth of colloidal heteronanocrystals.[7,19–21] The deposition modes for a secondary material onto a substrate are described with Franck–van der Merwe, Volmer–Weber, and Stranski–Krastanov models.[7,20] The three modes will result in continuous core–shell nanostructures, discontinuous core–branch nanostructures, and intermediate nanostructures, respectively.

Solid–solution interfacial energies and solid–solid interfacial energy with the respective materials are the underlying principles that determine which growth mode will be adopted. For example, a stable solid–solid interface with relatively unstable solid–solution interfaces favors the Franck–van der Merwe growth mode. The interfacial energies, determined by the lattice mismatch and interfacial bonding forces, are varied by the different types of facets, which offer a broad way to control the composition and overall morphology of the heteronanocrystals. For instance, gold nucleated and grew preferentially at a single tip of CdS nanorod, which was proposed to be the sulfur-rich end.[22] The formation of the CdS-gold heterostructures can also be understood as that the cation compulsive force between Au^{3+} and Cd^{2+} prevents the nucleation of gold on cadmium-rich surface. Furthermore, the coordination between Au and S^{2-} also stabilized the gold atoms. Therefore, the interfacial energy between gold and cadmium-rich surface is much more positive than that of the gold and sulfur-rich surface, which can be found of importance in the growth of many metal-chalcogenide heterostructures.[23,24] On the other hand, the role of anion compulsive force for the different interfaces during the growth of heterostructures has been seldom considered. The coordination environment, especially the coordination numbers of the interfacial atoms also need careful investigations.

Herein we present the facet-selective epitaxial growth of $NaYF_4$ on NaCl nanocubes. Both $NaYF_4$ and NaCl belong to $Fm\bar{3}m$ space group. The $NaYF_4$ nanocrystals have a calcium fluoride type structure, where Na^+ and Y^{3+} randomly form the face-centered cubic stacking, and F^- fill all of the tetrahedral sites. For NaCl, Na^+ form the same face-centered cubic stacking while Cl^- fill all the octahedral sites. The lattice mismatch between those two materials is 2.8%, and both materials contain Na^+. Therefore, the growth of $NaYF_4$ on NaCl is believed to follow the Franck–van der Merwe mode. However, structure studies reveal that the $NaYF_4$ nanocrystals preferentially grow at the eight corners of the NaCl nanocube instead of the six facets of the cube, indicating a preferential growth along the [111] direction. The resulting heterostructure is a core–cage structure instead of a core–shell structure. The NaCl nanocube then serves as a removable template for the growth of the nanocage structure. Theoretical calculations using density function theory (DFT) show that both the anion compulsive force and the coordination numbers of Y^{3+} determined the overall energy differences between (100)/(100) interface and (111)/(111) interface. The later interface was more stable than that of the former. Our study reveals the complexity at the solid–solid interfaces and suggests new ways of modifying the heteroepitaxial growth modes.

The heterostructure synthesis was conducted under an Ar atmosphere using a standard air-free Schlenk line technique. A one-pot synthesis was adopted to avoid the possible decomposition and dissolution of the NaCl nanocubes (see the Supporting Information). The formation of NaCl nanocubes was realized by the injection of HCl into the growth solution at 200°C (Scheme 1). The as-formed NaCl nanocubes sequentially served as the seeds for the heteroepitaxial

[*] Dr. F. Wang, Prof. Dr. L.-D. Sun, J. Gu, Y.-F. Wang, Dr. W. Feng, Y. Yang, Prof. Dr. C.-H. Yan
Beijing National Laboratory for Molecular Sciences, State Key Laboratory of Rare Earth Materials Chemistry and Applications, PKU-HKU Joint Laboratory in Rare Earth Materials and Bioinorganic Chemistry, Peking University
Beijing 100871 (China)
E-mail: sun@pku.edu.cn
yan@pku.edu.cn
Dr. F. Wang, Prof. Dr. J. F. Wang
Department of Physics, The Chinese University of Hong Kong
Shatin, Hong Kong SAR (China)
E-mail: jfwang@phy.cuhk.edu.hk

[**] This work was supported by the NSFC (No. 20971005, 20821091, and 20931160429), MOST of China (No. 2011AA03A407), and the Research Grants Council of Hong Kong (NSFC/RGC Joint Scheme, Ref. No. N_CUHK465/09, Project Code 2900339; Direct Allocation, Project Code 2060417).

Supporting information for this article is available on the WWW under http://dx.doi.org/10.1002/anie.201203069.

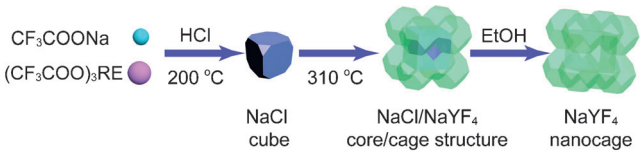

Scheme 1. The formation of a NaCl cube, a NaCl-$NaYF_4$ core–cage structure, and a $NaYF_4$ nanocage. RE = Y, Yb, Gd, Er. See the Supporting Information for details.

growth of $NaYF_4$ at 310 °C. The NaCl nanocubes inside the NaCl-$NaYF_4$ core–cage structures can be removed by ethanol, resulting in pure $NaYF_4$ nanocage structures.

To observe the formation of the NaCl nanocubes, 1 mL growth solution was extracted from the growth solution with a syringe at 200 °C with subsequent centrifugation and transmission electronic microscopy (TEM) measurement. The crystals had a cubic shape with the side length of about 18 nm (Supporting Information, Figure S1 a). High-resolution TEM (HRTEM) and an energy-dispersive spectrum (EDAX) confirmed the formation of NaCl (Supporting Information, Figure S1 b–d). The crystals were unstable under the electron beam and had low contrast under TEM. The pure $NaYF_4$ nanocage structures had an average side length of (30 ± 4) nm (Figure 1 a,b). They exhibited a fourfold symmetry with four $NaYF_4$ corners and one squared hollow-center (Figure 1 c). HRTEM images of two different sides of a single $NaYF_4$ showed the lattice fringes with a spacing of 0.200 nm, which can be indexed as (220) crystal planes of cubic-phase $NaYF_4$ (Figure 1 d,e). The lattice fringes of two diagonal particles were parallel, whereas the two adjacent particles are perpendicular. Owing to the fact that (220) planes were decussate squarely to each other, all of the $NaYF_4$ corners inside one nanocage took the same orientation. An electron diffraction pattern (Supporting Information, Figure S2) also indicated the same orientation of the $NaYF_4$ corners within one nanocage. To observe all of the eight nanocrystals in Figure 1 c, the TEM sample stage was tilted by 15°. At this angle, all of the nanocrystals exhibit the same set of lattice fringe of 0.302 nm, which corresponds well to (111) planes of cubic phase $NaYF_4$ (Supporting Information, Figure S3). A power X-ray diffraction (XRD) pattern (Figure 1 f) also confirmed the cubic-phase $NaYF_4$ structure (JCPDS: 06-0342) for the nanocages (Supporting Information, Table S1).

Three HAADF-STEM images (Figure 2) of an individual $NaYF_4$ nanocage were recorded at different observation angles to study their morphology and structures. Firstly, four $NaYF_4$ nanocrystals were recognized with fourfold symmetry when observing the [001] axis (Figure 2 a). One-eighth of each nanocrystal was missing according to the relative contrast of the image, leaving a cubic vacancy area located in the center. When observed in the [011] direction, six nanocrystals were revealed. The middle two were located at the nearest side facing to observer, while the missing two nanocrystals were concealed behind them at the back. Observing in the [111] direction, seven nanocrystals were displayed with threefold symmetry. The one in the center, which is located at the nearest corner facing to the observer, was surrounded by six others coming from two crystal planes. The missing one

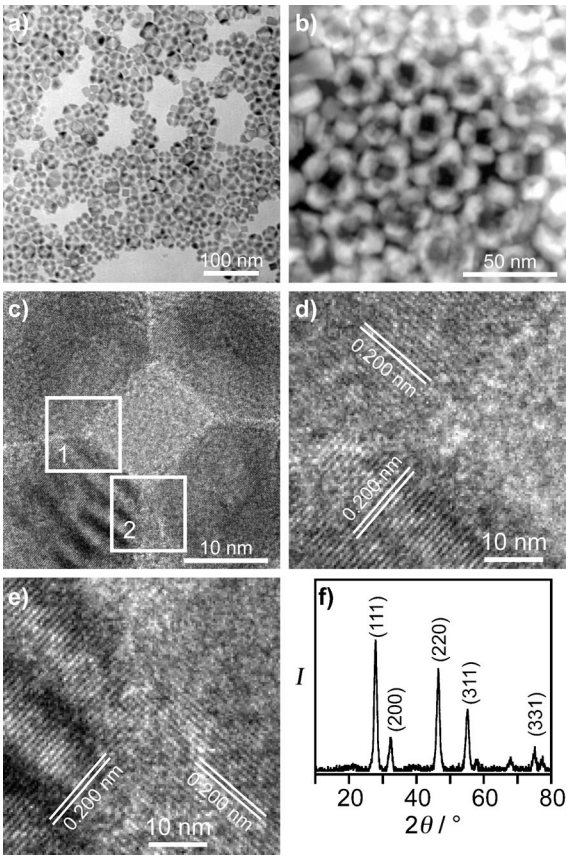

Figure 1. Structure of $NaYF_4$ nanocages. a) TEM image; b) high-angle annular dark-field-scanning TEM (HAADF-STEM) image; c) TEM image of a single nanocage; d), e) HRTEM images recorded from the regions indicated by panels 1 and 2, respectively, in (c); f) XRD patterns of a $NaYF_4$ nanocage.

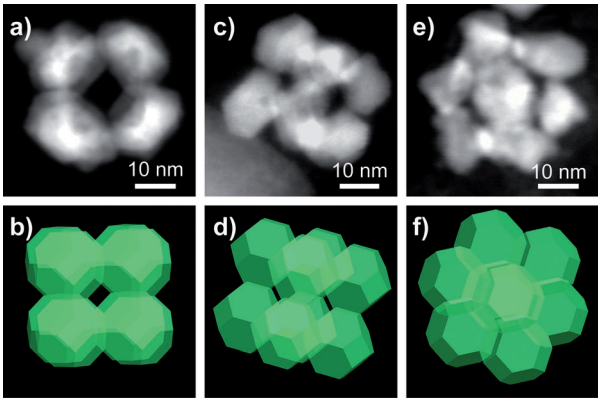

Figure 2. HAADF-STEM images and corresponding models of an individual $NaYF_4$ nanocage. a), c), e) HAADF-STEM images observed in [001], [011], and [111] directions, respectively. b), d), f) Corresponding 3D models.

should be located at the farthest point of the [111] cage. To observe the overall rotating process, a nanocage in the [001] direction was rotated horizontally from 0 to 45° to reveal the image in the [011] direction. Then, a vertical rotation from 0 to 28° gave an image that was close to the observation in the [111] direction (Supporting Information, Figure S4).

Both NaCl and $NaYF_4$ are face-centered cubic structures. Their lattice constants are 0.564 nm and 0.545 nm, respectively. Owing to the low solubility of NaCl in acetone, this solvent was used instead of ethanol to precipitate the product after the growth. Such treatment retained the NaCl nanocubes, which are located in the center of the nanocage (Figure 3a; Supporting Information, Figure S5). The lattice

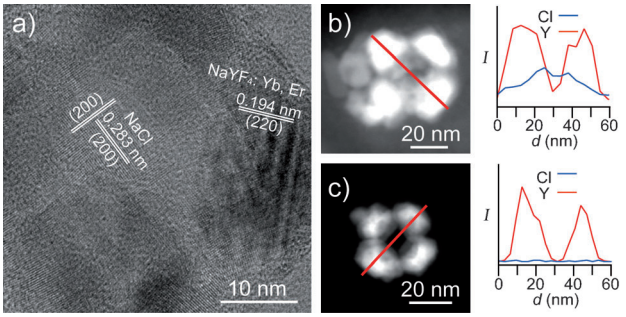

Figure 3. a) HRTEM image of a NaCl-$NaYF_4$ core–cage structure. b), c) HAADF-STEM image and elemental line profile of b) a NaCl-NaYF core–cage structure and c) a $NaYF_4$ nanocage.

fringes in the center can be indexed to (200) crystal planes of NaCl. Elemental line profiles across the NaCl-$NaYF_4$ core–cage structure and $NaYF_4$ nanocage were recorded across the center region of the nanocrystals along the direction that was parallel to diagonal of the cubic structure. For the NaCl-$NaYF_4$ core–cage structure, the Y trace has two peaks, whereas the Cl trace has only one peak (Figure 3b). The position of the valley between the two peaks in the Y traces corresponds well to the peak position of the Cl trace, suggesting that the NaCl nanocube was in the middle of the nanostructure. As for $NaYF_4$ nanocage (Figure 3c), the line profiles revealed that the Y trace still has two peaks whereas Cl shows no signal, indicating the completely removal of the NaCl nanocube with a simple ethanol treatment. The $NaYF_4$ nanocages doped with Yb^{3+} and Er^{3+} behave a relative increased transition of $^2H_{11/2}$ and $^4S_{3/2}$ to $^4I_{15/2}$ (Supporting Information, Figure S6), and an increased green to red emission ratio of 2.27 was obtained (0.53 for nanospheres).[25]

The aforementioned studies of the NaCl-$NaYF_4$ core–cage structure indicate a preferential heteroepitaxial growth of $NaYF_4$ on the eight corners of the NaCl nanocubes. The growth is therefore along the [111] direction. To elucidate the facet selectivity, we performed DFT calculations on the interfacial energy between the (100) and (111) interfaces of $NaYF_4$ and NaCl (Supporting Information, DFT calculations). NaCl has a sodium-rich (111) surface and a chlorine-rich (111) surface. $NaYF_4$ also has a cation-rich (100) surface and an anion-rich (100) surface. Therefore, there are four different interfaces, dented interfaces **A**, **B**, **C**, and **D**, respectively (Supporting Information, Scheme S1). For each case, we set up a slab containing three layers of NaCl and three layers of $NaYF_4$. The distributions of Na^+ and Y^{3+} in the $NaYF_4$ crystals were randomly disordered. To minimize the calculation process, we selected one Na/Y distribution state for the calculation. 10 Å vacuum layers were set up on the every slab.

The interfacial energy can be determined by the deducing the energies of NaCl and $NaYF_4$ in the bulk crystals and the respective energies of top and bottom surfaces. The energies of the polar surfaces, the NaCl (111) surface and $NaYF_4$ (100) surface, were calculated based on a reported method.[26] The interfacial energies were then plotted against $E_{(Na)}$ (Supporting Information, Figure S7), where $E_{(Na)}$ was the chemical potential of the reservoir of Na atoms. The exact value of $E_{(Na)}$ cannot be determined in the reaction system. Because no other species were found besides NaCl and $NaYF_4$, we set the range from −5.088 eV to −1.458 eV (Supporting Information, DFT calculations). The promising value of $E_{(Na)}$ in the reaction system was located in the middle range between −5.088 eV and −1.458 eV.

DFT calculations showed that the interface **C** has the lowest energy with respect to the promising value of $E_{(Na)}$. A close observation of the interfacial structure after relaxation reveals that both the anion compulsion force and the coordination numbers of Y^{3+} ions were important to the stability of the interface (Figure 4). In the initiate state, the Cl^- ions were directly contacted with F^- ions at interface **A** (Supporting Information, Scheme S1a), which pushes the F^- back into the anion layer of the $NaYF_4$ crystals and the Cl^- back into the interior of NaCl crystals (Figure 4a). In the relaxed state, the distance between Cl^- and F^- ions at interface **A** is 3.38 Å. The newly formed F^-–Na^+ layer was crowed and unstable. A similar case is interface **D**, giving close distances between Cl^- and F^- ions in the initiate state (Supporting Information, Scheme S1d). After relaxation, the distance between the interfacial Cl^- and F^- was only 2.99 Å, leading to a strong Coulomb repulsion (Figure 4d). On the other hand, the compulsive force between Cl^- and F^- ions was minimized at interface **B** or **C** (Supporting Information, Scheme S1b,c), with the tradeoff of low coordination number of Y^{3+} ions at the interface. The coordination number of Y^{3+} ions in $NaYF_4$ crystal is eight, with 4 F^- ions at the upper layer and 4 F^- ions at the lower layer. At interface **B**, regarding the (100) interface, the $NaYF_4$ side still offer 4 F^- ions, while the NaCl side can only offer one Cl^- as the coordination anion (Figure 4b). The interface with low coordination number of Y^{3+} ion is also unstable. On the other hand, the coordination number of the Y^{3+} ion at interface **C** is seven (Figure 4c), which was close to the original coordination environment in $NaYF_4$. The interfacial energy of interface **C** is therefore the lowest at the possible $E_{(Na)}$ range. The DFT calculations showed that the interface **C** was the most promising to stabilize during the heteroepitaxial growth of $NaYF_4$ on NaCl. Therefore, the $NaYF_4$ preferentially grew along [111] direction of the NaCl nanocubes. The calculation results were in good accordance with the aforementioned structural studies.

The synthesis can be extended to other $NaREF_4$ nanocages, such as $NaGdF_4$ (Supporting Information, Figure S8). $NaGdF_4$ also shared similar crystallographic parameters with that of NaCl (Supporting Information, Table S1). The eight-in-one $NaGdF_4$ nanocages, with an average size of about 20 nm, also exhibit the fourfold symmetry. HRTEM image reveals that the (111) lattice fringe with the spacing of

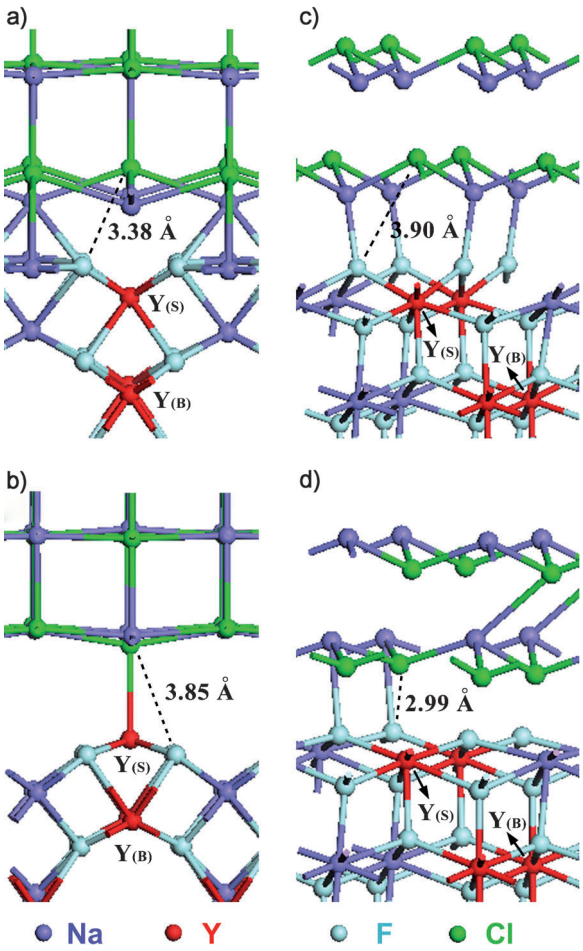

Figure 4. Diagrams showing the interfacial structures after relaxation. a) Interface **A**: (100) NaCl facet and fluorine-rich (100) $NaYF_4$ facet. b) Interface **B**: (100) NaCl facet and cation-rich (100) $NaYF_4$ facet. c) Interface **C**: Sodium-rich (111) NaCl facet and (111) $NaYF_4$ facet. d) Interface **D**: Chlorine-rich (111) NaCl facet and (111) $NaYF_4$ facet. The interfaces **A** and **B** were viewed in the [010] direction; interfaces **C** and **D** in the [1-10] direction.

0.317 nm of cubic $NaGdF_4$. The cage structure using NaCl as the template is quite general for $NaREF_4$, and may promising for other nanocrystals with a similar crystallographic parameters and a comfortable interface.

In summary, a one-pot solution route to produce high-quality $NaYF_4$-NaCl core–cage structures and $NaYF_4$ nanocages has been developed. The core–cage structures resulted by the facet-selective heteroepitaxial growth of $NaYF_4$ on NaCl nanocubes. The energy difference in interfaces of $NaYF_4$ and NaCl directed the $NaYF_4$ grew at eight corners of the NaCl nanocubes to form an eight-in-one cage structure instead of a core–shell structure. The NaCl nanocubes functioned as the structure-directing template, which could be removed after the heteroepitaxial growth. DFT calculations showed that the interfacial energies were decided by the anion compulsion and the coordination numbers of interfacial Y^{3+} ions. Our study on the ionic behaviors of the $NaYF_4$–NaCl interface is an important step in understanding the heteroepitaxial growth and suggests new ways of synthesizing heterostructures. Hollow structured luminescent nanocrystals may not only lead to new luminescent behaviors but also can find potential applications in targeted drug delivery.

Received: April 21, 2012
Published online: July 17, 2012

Keywords: colloidal nanocrystals · crystal growth · density functional calculations · heteroepitaxy · interfacial energy

[1] D. J. Milliron, S. M. Hughes, Y. Cui, L. Manna, J. B. Li, L.-W. Wang, A. P. Alivisatos, *Nature* **2004**, *430*, 190–195.
[2] T. Mokari, E. Rothenberg, I. Popov, R. Costi, U. Banin, *Science* **2004**, *304*, 1787–1790.
[3] H. Yu, M. Chen, P. M. Rice, S. X. Wang, R. L. White, S. H. Sun, *Nano Lett.* **2005**, *5*, 379–382.
[4] P. D. Cozzoli, T. Pellegrino, L. Manna, *Chem. Soc. Rev.* **2006**, *35*, 1195–1208.
[5] C. Xue, J. E. Millstone, S. Y. Li, C. A. Mirkin, *Angew. Chem.* **2007**, *119*, 8588–8591; *Angew. Chem. Int. Ed.* **2007**, *46*, 8436–8439.
[6] D. S. Wang, Y. D. Li, *J. Am. Chem. Soc.* **2010**, *132*, 6280–6281.
[7] L. Carbone, P. D. Cozzoli, *Nano Today* **2010**, *5*, 449–493.
[8] K. A. Abel, J.-C. Boyer, F. C. J. M. van Veggel, *J. Am. Chem. Soc.* **2009**, *131*, 14644–14645.
[9] H. Zhang, Y. Li, I. A. Ivanov, Q. Qu, Y. Huang, X. F. Duan, *Angew. Chem.* **2010**, *122*, 2927–2930; *Angew. Chem. Int. Ed.* **2010**, *49*, 2865–2868.
[10] F. Tao, M. E. Grass, Y. W. Zhang, D. R. Butcher, J. R. Renzas, Z. Liu, J. Y. Chung, B. J. S. Mun, M. Salmeron, G. A. Somorjai, *Science* **2008**, *322*, 932–934.
[11] B. K. Lim, M. J. Jiang, P. H. C. Camargo, E. C. Cho, J. Tao, X. M. Lu, Y. M. Zhu, Y. N. Xia, *Science* **2009**, *324*, 1302–1305.
[12] F. Wang, C. H. Li, L.-D. Sun, H. S. Wu, T. Ming, J. F. Wang, J. C. Yu, C.-H. Yan, *J. Am. Chem. Soc.* **2011**, *133*, 1106–1111.
[13] B. Z. Tian, X. L. Zheng, T. J. Kempa, Y. Fang, N. F. Yu, G. H. Yu, J. L. Huang, C. M. Lieber, *Nature* **2007**, *449*, 885–889.
[14] J. Y. Tang, Z. Y. Huo, S. Brittman, H. W. Gao, P. D. Yang, *Nat. Nanotechnol.* **2011**, *6*, 568–572.
[15] Y.-L. Chueh, C.-H. Hsieh, M.-T. Chang, L.-J. Chou, C. S. Lao, J. H. Song, J.-Y. Gan, Z. L. Wang, *Adv. Mater.* **2007**, *19*, 143–149.
[16] J. Lin, Y. Huang, Y. Bando, C. C. Tang, C. Li, D. Golberg, *ACS Nano* **2010**, *4*, 2452–2458.
[17] F. Wang, R. R. Deng, J. Wang, Q. X. Wang, Y. Han, H. M. Zhu, X. Y. Chen, X. G. Liu, *Nat. Mater.* **2011**, *10*, 968–973.
[18] A. Xia, Y, Gao, J. Zhou, C. Y. Li, T. S. Yang, D. M. Wu, L. M. Wu, F. Y. Li, *Biomaterials* **2011**, *32*, 7200–7208.
[19] E. Bauer, J. H. van der Merwe, *Phys. Rev. B* **1986**, *33*, 3657–3671.
[20] F.-R. Fan, D.-Y. Liu, Y.-F. Wu, S. Duan, Z.-X. Xie, Z.-Y. Jiang, Z.-Q. Tian, *J. Am. Chem. Soc.* **2008**, *130*, 6949–6951.
[21] M. Casavola, R. Buonsanti, G. Caputo, P. D. Cozzoli, *Eur. J. Inorg. Chem.* **2008**, 837–854.
[22] J. Yang, H. I. Elim, Q. B. Zhang, J. Y. Lee, W. Ji, *J. Am. Chem. Soc.* **2006**, *128*, 11921–11926.
[23] T. Mokari, C. G. Sztrum, A. Salant, E. Rabani, U. Banin, *Nat. Mater.* **2005**, *4*, 855–863.
[24] A. Figuerola, M. van Huis, M. Zanella, A. Genovese, S. Marras, A. Falqui, H. W. Zandbergen, R. Cingolani, L. Manna, *Nano Lett.* **2010**, *10*, 3028–3036.
[25] S. Heer, K. Kömpe, H.-U. Güdel, M. Haase, *Adv. Mater.* **2004**, *16*, 2102–2105.
[26] S. B. Zhang, S.-H. Wei, A. Zunger, *Phys. Rev. B* **2001**, *63*, 075205.

